Fuel 381 (2025) 133559

Contents lists available at ScienceDirect

Fuel

journal homepage: www.elsevier.com/locate/fuel

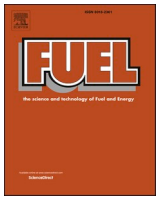

Full Length Article

Optimization of anode porous transport layer's coating for enhanced proton exchange membrane electrolyzer cells

Xiuyue Wang [a], Jiexin Zou [b], Zhen Zhang [c,*], Cenkai Zhao [a], Min Wang [a,*], Mingbo Wu [a,*]

[a] College of New Energy, China University of Petroleum (East China), Qingdao 266580, China
[b] Qingdao Haier Smart Technology R&D Co., Ltd., Qingdao 266101, China
[c] Shenzhen Center Power Technology Co., Ltd., Shenzhen 518120, Guangdong, China

ARTICLE INFO

Keywords:
PEMEC
Porous transport layer
Electrodeposition
Pt coating
Mass transfer

ABSTRACT

The anode porous transport layer (PTL) is a key component in proton exchange membrane electrolyzer cells (PEMECs), which directly affects the cell's overall electrochemical performance. Currently, Ti felt is one of the most suitable materials for anode PTL, although a surface coating layer is necessary due to the oxidized passivation film on the surface of the Ti felt, which leads to high interfacial contact resistance. Therefore, rational design and the appropriate coating strategy are crucial. In this study, the electrodeposition technique was employed to fabricate Pt coating layers with different thicknesses on Ti felt-based PTLs and its impact on PEMEC's performance was systematically investigated. The results showed that the optimized Pt coating can maximize performance by improving the PTL/catalyst layer (CL) interface. Interestingly, high Pt coating (≥0.7 μm) resulted in lower cell performance, which was attributed to increased mass transfer resistance and restricted two-phase flow caused by excessive coating. To address this issue, ordered water channels on the coated PTL were constructed via the laser ablation technique. Mass transfer overpotential had been reduced by more than 40 % due to the introduction of water channels, and the bubble transfer behavior was monitored in-situ via a transparent electrolyzer. In addition, the durability of PEMEC was further confirmed through aging tests, highlighting the positive effect of the Pt coating. This study provides an experimental basis for the optimization strategy of PTL's coating and valuable guidance for other energy conversion systems, such as fuel cells and CO_2 electrolyzers.

1. Introduction

Hydrogen energy plays a crucial role in addressing the climate crisis and maintaining national energy security, making it an essential part of the energy transition [1–6]. In particular, the production of green hydrogen is one of the key issues limiting the sustainable expansion of hydrogen energy. Currently, the cost of green hydrogen production remains relatively high, posing a major challenge [7]. Utilizing renewable energy for power generation is an effective way to reduce costs, but it requires efficient and technological support [8,9]. In this regard, proton exchange membrane electrolyzer cells (PEMECs) have a rapid response time on the order of microseconds, effectively compensating for the intermittency and instability of renewable energy generation. It is a critical technology that requires vigorous development [10–12].

The porous transport layer (PTL) is one of the key components of PEMECs, providing channels for the transport of water from the bipolar plate (BP) to the catalyst layer (CL), and also for the gas transport from the CL to the BP, as well as conducting electrons and heat between the flow field and the catalyst-coated-membrane (CCM) [13]. During operation, the anode region of the PEMECs is in an oxygen-rich state, which imposes high demands on the material of the anode's PTL [14,15]. Ti is renowned for its excellent electrical conductivity and good corrosion resistance. Consequently, sintered Ti plates [16–18], Ti meshes [19,20], Ti foils [21,22], Ti felts [23–25] have been widely used as anode PTLs in PEMECs. In practical applications, these materials still exhibit certain limitations. For instance, high thickness of sintered Ti plates results in large volume and low conductive ability [26]. The rough surface can easily damage the CCM [27]. Additionally, sintered Ti plates are relatively dense with small pores, increasing mass transfer resistance [28]. The large pores of Ti meshes often lead to a reduced contact area with the CL, which in turn impedes the catalyst's full potential from being realized [20]. Uneven stress distribution between the Ti mesh and

* Corresponding authors.
E-mail addresses: zhangzhen@vision-batt.com (Z. Zhang), minwang@upc.edu.cn (M. Wang), wumb@upc.edu.cn (M. Wu).

https://doi.org/10.1016/j.fuel.2024.133559
Received 8 July 2024; Received in revised form 23 October 2024; Accepted 25 October 2024
0016-2361/© 2024 Elsevier Ltd. All rights are reserved, including those for text and data mining, AI training, and similar technologies.

the membrane electrode assembly (MEA) can cause irreversible mechanical damage to the MEA, reducing its lifespan [29]. Ti foils are not common in PEMEC, they act as PTLs mainly by perforating the surface to form gas–liquid channels. The extremely thin Ti foils (typically 20–30 μm) are beneficial for reducing the volume of PEMECs and lowering contact resistance [22]. However, the thin structure has a negative effect on its mechanical strength. It should be noted that the mechanical properties of thin Ti foils cannot meet the requirements for PEMECs with high hydrogen outlet pressures [30,31]. In contrast, Ti felts offer better control of thickness and porosity, and when used in PEMECs, the thickness of Ti felts is kept in the hundred-micron range, with the porosity ranging from 30 % to 50 % [32]. This structure is more conducive to maintaining a stable, two-phase transport process within the PEMECs. However, the surface of Ti felts is prone to forming an oxide passivation film, resulting in increased contact resistance and reduced hydrogen production efficiency [33,34]. To address these challenges, rational design of coating technology is crucial to improving PEMEC's performance.

Currently, PEMECs are required to operate for tens of thousands of hours, especially large-scale equipment like GW-scaled PEMECs, where continuous high efficiency and stability are necessary [35,36]. An appropriate coating strategy can improve the performance and durability of PEMECs. Liu et al. [37] conducted a study on different noble metal coatings and found that after 4000 h of durability tests, Pt and Ir coatings showed excellent protective effects. Considering the scarcity of global Ir resources [38], Pt coatings are more cost-effective compared to Ir coatings. Kang et al. [39] compared the performance of different coating techniques. They found that the surface of the gold-plated coating obtained by plasma sputtering deposition exhibited noticeable cracks compared to the samples obtained by electrodeposition. The advantages of the electrodeposition treatment were also revealed by polarization performance and durability tests. Physical vapor deposition (PVD), another commonly used deposition techniques, can precisely control the thickness, composition, and microstructure of the coating. However, PVD requires larger initial investment costs. Electrolyzers require appropriate PTL coverage. To meet this demand, PVD processes necessitate oversized equipment chambers. It results in disproportionately large Pt target areas and extremely high costs, making it unsuitable for MW-scaled and GW-scaled electrolyzers. Compared to the PVD, traditional electrodeposition technology, although slightly less precise, is suitable for large-area deposition and provides a more uniform coating. The thickness of electrodeposited coatings is closely related to durability and cost, but research in this area is relatively scarce.

This study rationally designed and electrodeposited Pt coatings on Ti felts as a substrate, providing a protective effect similar to Ir coatings but with a more cost-effective advantage. By controlling the electrodeposition time, the thickness of the Pt coating was precisely controlled. Through single-cell tests, the critical amount of the coating layer (optimal coating thickness) was successfully defined. Beyond this optimal coating thickness, no performance improvement was observed. Overpotential analysis showed that at high current densities, the main reason for the limited performance improvement is that the thicker Pt coating ($\geq$0.7 μm) blocks the pores in the Ti felt, restricting the two-phase transport in the PTL. Subsequent construction of water channels on Ti felt-based PTL effectively solves this issue, providing a simple and feasible solution to enhance mass transfer. Additionally, aging tests was carried out, furthermore, the polarization performance decay of the Ti felt-based PTL before and after coating was compared, confirming the positive effect of the coating on PEMEC's durability.

2. Experimental section

2.1. PTL's treatment

2.1.1. Materials and pretreatment

The PTLs used in this study were purchased from China Titanium Guochuang (Qingdao) Technology Co., Ltd. with a thickness of approximately 250 μm ± 5 μm. The Ti felt-based PTL was denoted as ZT250. The cross-sectional scanning electron microscopy (SEM) image is shown in Fig. S1 (a). Before coating, all PTLs underwent a cleaning process to remove surface contaminants [25]. Specifically speaking, the PTLs were first immersed in ultrapure water and heated to 80 °C for 15 min. Next, they were placed in an ultrasonic bath with 2-propanol and acetone for another 15 min. Finally, the PTLs were rinsed twice with deionized water at 80 °C for 15 min each and then air-dried at room temperature overnight.

2.1.2. Electrodeposition of Pt coating

The electrolyte was prepared using chloroplatinic acid (Aldrich), sulphuric acid (Sinopharm Chemical Reagent Co., Ltd.) and ultrapure water. For electroplating, a Ru-Ir Ti mesh was used as the anode and a Ti felt-based as the cathode. A 0.1 μm thick layer was electrodeposited within 5 min at a current density of 30 mA cm^{-2}, as demonstrated by the SEM and mapping images of ZT250-Pt0.1 in Fig. S1(b). Under constant current conditions, the coating thickness of the PTL was controlled by varying the electrodeposition time. The electrodeposited samples were denoted as ZT250-Pt0.1, ZT250-Pt0.3, ZT250-Pt0.5, and ZT250-Pt0.7 (the sample details are shown in Table S1).

2.1.3. Laser ablation

A VLS3.60 machine (Universal Laser Systems, Inc.) was employed to create ordered water channels on the surface. Laser power of 35 W at a speed of 5 % was applied to fabricate straight-through pores on the Ti felt-based PTL surface. The number of pulses per inch (PPI) of the laser system is set to 500. The diameter of the pores was approximately 500 μm, and the center-to-center distance between adjacent pores was 1 mm. It was obtained by repeating the process 100 times. The porosity caused by the straight-through pores was calculated to be about 20 %. After the laser ablation, cleaning was performed with reference to the post-processing method of Lee et al. [40]. The treated sample was denoted as ZT250-Pt0.7-Waterchannel.

2.2. Preparation of CCMs

In this experiment, Nafion115 was chosen as the proton exchange membrane. Before preparing the CCM, activation of Nafion was performed [41,42]. The specific steps were as follows: first, the Nafion 115 was treated with a 5 wt% aqueous H_2O_2 solution at 80 °C for 1 h to remove organic impurities. Then, the membrane was immersed in a 1.0 M H_2SO_4 aqueous solution at 80 °C for 1 h to promote protonation. Next, the membrane was heat-treated in ultrapure water at 80 °C for 1 h to remove residual acid and hydrogen peroxide. Finally, the membrane was repeatedly rinsed with ultrapure water.

CCMs were prepared using the UAM4000 ultrasonic spaying system (Hangzhou Cheersonic Ultrasonic Equipment Co., Ltd.), with 95 wt% IrO_2 (Ningbo Zhongke Innovation Energy Technology Co., Ltd.) and 50 wt% Pt/C (TANAKA Kikinzoku Korea Co., Ltd.) as the anode and cathode catalysts, respectively. The slurry formulation followed the method published by Kang et al. [11], where the catalyst powders were evenly dispersed in a solvent mixture of n-propanol and ultrapure water, with a certain amount of Nafion D520 added as a binder. The water/alcohol volume ratio was 1.3. For the anode slurry, the ionomer/catalyst mass ratio was 0.24, while for the cathode slurry, it was 0.45. Ultrasonic dispersion was conducted in an ice bath, with the anode catalyst layer slurry undergoing 1 h of ultrasonication and the cathode catalyst layer slurry undergoing 30 min of ultrasonication [43]. After ultrasonic dispersion, the slurry was evenly sprayed onto both sides of Nafion 115. The catalyst loading for the anode was determined to be approximately 2 mg_{IrO2} cm^{-2}, and for the cathode, it was approximately 0.5 mg_{Pt} cm^{-2}. The cross-sectional image of the CCM is shown in Fig. S1(c).

2.3. Electrolyzer assembly

The MEA is a crucial component of PEMECs, comprising PTLs and CCM. TGP-H 060 carbon papers (Toray Industries, Inc.) with a thickness of 190 μm were used as cathode PTLs, while Ti felts with different coating thicknesses were used as anode PTLs. A schematic diagram of the electrolyzer's structure is shown in Fig. 1 (a). Single-cell test was conducted using dual-sided Pt-coated plates with an active area of 4 cm^2 and single serpentine flow channel. A torque of 3 N m was uniformly applied to each of the 4 bolts.

2.4. Electrochemical measurements

2.4.1. PEMEC test

The PEMEC test system is shown in Fig. 1(b). Throughout the tests, the system temperature and inlet water temperature were maintained at 80 ℃, with ultrapure water circulated in the anode chamber at a flow rate of 40 mL min^{-1}.

Before conducting polarization curve and electrochemical impedance spectroscopy (EIS) tests, the MEA needed to be activated in the electrolyzer. The break in procedure [25] was as follows: 1) hold the cell at a current density of 0.2 A·cm^{-2} for 30 min; 2) continue running at a current density of 1.0 A·cm^{-2} for another 30 min; 3) maintain at 1.7 V until the current change is less than 1 % per hour. After activation, polarization performance test was conducted using a constant voltage method, increasing the voltage from 1.3 V to 2.4 V with an increment of 0.05 V. Each voltage was held for 5 min. The polarization curve measurements were completed using a BT-2018D power supply (Hubei LANBO New Energy Equipment Co., Ltd.). For EIS measurement, an electrochemical workstation (Gamry, Interface 5000) was employed using the Galvanostatic EIS mode. The test current was set to 1 A, the current perturbation was 5 % of the test current, and the frequency range was from 100 kHz to 0.1 Hz.

2.4.2. Transparent electrolyzer test

The transparent electrolyzer test system, as shown in Fig. S2, is constructed similarly to the PEMEC test system. The distinction lay in the use of an electrolyzer featuring a transparent plate on the anode side in this setup. Besides, a KoPa Capture Ver9.9 optical microscope (Guangzhou OSTEC Electronic Technology Co., Ltd.) was utilized for in-situ observation of bubble changes. During the tests, ultrapure water was still circulating in the anode chamber at a flow rate of 40 mL min^{-1}. Bubble generation was observed at a current density of 3 A cm^{-2} for the ZT250-Pt0.7 and ZT250-Pt0.7-Waterchannel acting as the anode PTL, respectively.

2.4.3. A three-electrode aging test

Aging tests were conducted in the aqueous H_2SO_4 solution (pH = 2) [44,45]. Electrochemical measurements were carried out using an electrochemical workstation (DongHua Analytical DH7003), employing a three-electrode system. The counter electrode (CE) was a Pt sheet, and the reference electrode (RE) was an Ag/AgCl electrode. The reference electrodes were calibrated according to established literature [46,47] methods prior to use. Comprehensive experimental procedures are provided in the Supporting Information. The tested sample served as the working electrode (WE), with an effective area of 4 cm^2. In the chronopotentiometric mode, the current was set constant at 10 mA for 100 h of aging tests.

2.5. Overpotential analysis

The electrolyzer voltage (E_{cell}) is mainly composed of reversible voltage (E^0(p, T)), ohmic overpotential (η_{ohmic}), kinetic overpotential (η_{kin}), and mass transport overpotential (η_{mt}) [48,49], which can be expressed as:

$$E_{cell} = E^0(p,T) + E_{ohmic} + E_{kin} + E_{mt}$$

Under atmospheric pressure conditions, the reversible voltage (E^0(p, T)) is related to the actual operating temperature of the electrolyzer and can be defined as:

$$E^0(p,T) = 1.2291 - 0.0008456\ (T - 298.15)$$

where T is the electrolyzer temperature (K).

η_{ohmic} is calculated using high-frequency resistance (HFR) and can be expressed as:

$$\eta_{ohmic} = i{\cdot}HFR$$

where i is the applied current density (A cm^{-2}), and HFR is measured by fitting x intercept from the Nyquist plot (Ω cm^2).

In the water electrolysis process, both the hydrogen evolution reaction (HER) and the oxygen evolution reaction (OER) occur, and OER is considered the rate-determining step. The η_{kin} and η_{mt} caused by OER are much greater than those caused by HER. Therefore, in this study, only the η_{kin} and η_{mt} caused by OER, as well as the η_{ohmic} of the entire electrolyzer, are considered. Based on this, η_{kin} can be expressed as:

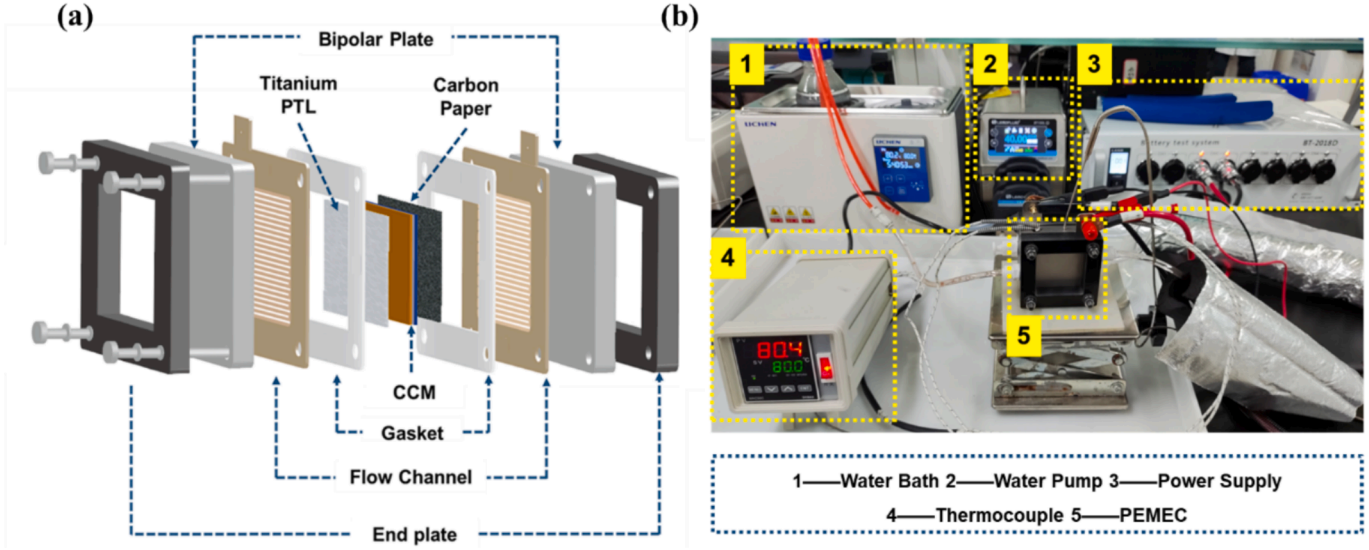

Fig. 1. Schematic diagram of (a) PEMEC and (b) PEMEC test system.

$$\eta_{kin} = b\log\left(\frac{i}{i_0}\right)$$

where b is the Tafel slope (mV dec^{-1}), i is the applied current density (A cm^{-2}), and i_0 is the exchange current density (A cm^{-2}).

η_{mt} can be expressed as:

$$E_{mt} = E_{cell} - E^0(p,T) - E_{ohmic} - E_{kin}$$

2.6. Structural characterization

SEM was performed using a Hitachi Regulus SU8100 to observe the morphology of the CCM's cross-section and the PTL, while Zeiss Sigma 300 was used for EDS analysis of the coated PTL to determine element distribution. The coating thickness of ZT250-Pt0.1 was observed using a Helios 600i from FEI, with carbon used as a protective element during testing. Keyence VR-3000 was used to observe the 3D profiles of the PTL before and after coating, and the surface average roughness (R_a) was calculated. The conductivity of the PTL before and after electrodeposition was tested using a four-probe resistivity tester, model ST-2722, from Suzhou Lattice Electronics Co., Ltd. X-ray diffraction (XRD) was conducted using Cu Kα radiation (λ = 1.5418 Å) with a Rigaku Ultima IV to characterize the crystal structure of the samples. X-ray photoelectron spectroscopy (XPS) was performed using a Thermo Scientific K-Alpha to study the effect of the coating on durability.

3. Results and discussion

3.1. Characterization of PTL's coating

Fig. 2(a) shows the key components inside the PEMECs, where the PTL acts as a bridge for gas–liquid transport between the BP and the CL. As shown in the SEM and mapping image in Fig. 2(b), the surface structure of ZT250 was relatively regular, and the Ti wire's diameter was around 25 μm. In addition to the Ti element, a large amount of oxygen element was also distributed on the surface of ZT250, which was due to its surface oxidation in the air [37]. After electrodeposition, the Pt element was uniformly distributed (Fig. 2(c)), not only on the substrate's surface but also covering the Ti wires inside the pores. Fig. S4 presents SEM images and mapping of the Ti felt after PVD coating. The comparison clearly showed that the PVD coating primarily affects the surface layer, with minimal Pt observed within the internal pores of the Ti felt. This explains why electrodeposition is superior to the PVD. The effect of electrodeposition coating on the R_a was investigated by a 3D profilometer. Compared with ZT250 (Fig. 2(d)), the surface of ZT250-Pt0.5 (Fig. 2(e)) exhibited a smoother three-dimensional morphology. R_a was calculated by randomly selecting 40 straight lines on the surfaces of ZT250 and ZT250-Pt0.5, and the results are shown in Fig. 2(f) and (g), respectively. The coating treatment reduced the R_a values.

Fig. 3 shows the XRD patterns of PTL with different coating thickness. The grey lines represent the XRD results of ZT250, which showed the main peaks of (100), (002), (101), (102), (110), (103), (112), and (201) at 2θ angles of 35.1°, 38.1°, 40.2°, 53.0°, 62.9°, 70.7°, 76.2°, and 77.4°, respectively. The results of ZT250 are in accordance with the Ti standard diffraction file (PDF# 44-1294). The other samples with Pt coatings have increased (111), (200), and (220) diffraction peaks compared to ZT250. Their main peaks are distributed at 2θ angles of 39.8°, 46.2°, 67.5°, corresponding to the standard diffraction file for Pt (PDF# 04–0802). The (111), (200), and (220) diffraction peaks were more prominent, and the peak intensity increased with the increase in coating thickness. By observing the enlarged XRD spectra in Fig. 3(b), it can be seen that the peak width of the Pt (111) peak is small, indicating that the size of the Pt crystal on the PTL surface is larger. According to the peak widths of the corresponding XRD peaks, the size of the crystal can also be determined by using Scherrer's formula [50]. The specific formula is shown below:

$$D_{hkl} = N_d = \frac{k\lambda}{\beta\cos\theta}$$

where D_{hkl} is the grain diameter along the direction perpendicular to the crystal plane (*hkl*), k is Scherrer's constant (usually 0.89), λ is the wavelength of incident X-rays (Cuka wavelength 0.15406 nm), θ is the Bragg angle of diffraction (°), and β is the half-peak width of the diffraction peak (rad).

The size of the Pt particles was calculated to be roughly 20 nm after the fit. Due to the lower concentration of Pt relative to the Ti substrate, the diffraction peaks corresponding to the (3 1 1) and (2 2 2) crystal planes of Pt were less pronounced, appearing as weaker signals amidst the intense peaks of the Ti substrate. Nonetheless, a trend towards increasing coating thickness can still be seen by observing the change in the intensity of the diffraction peaks.

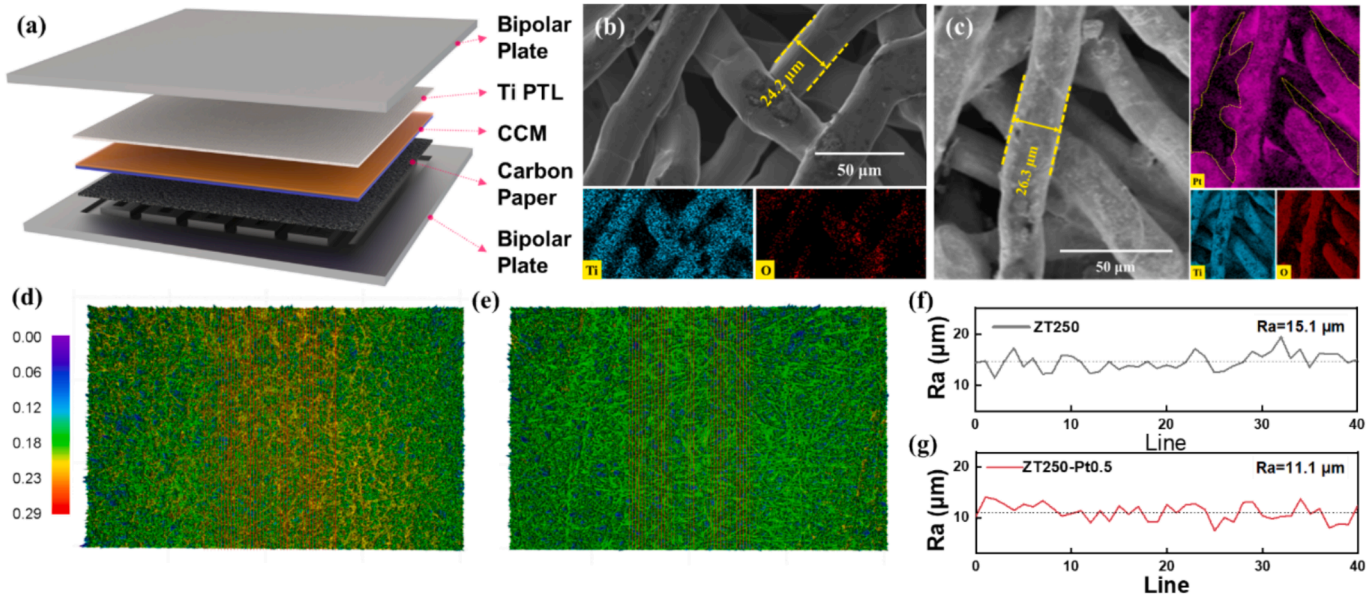

Fig. 2. (a) Schematic diagram of PEMEC's key components; surface morphology and element distribution of (b) ZT250 and (c) ZT250-Pt0.5; surface profile of (d) ZT250 and (e) ZT250-Pt0.5; average surface roughness of (f) ZT250 and (g) ZT250-Pt0.5.

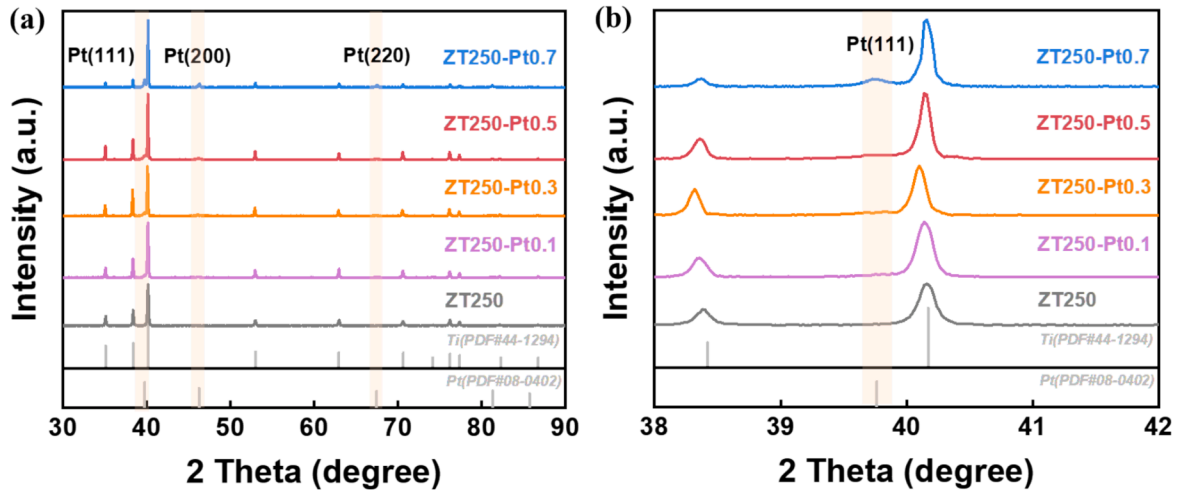

Fig. 3. (a) XRD patterns of PTL with different coating thickness; (b) enlarged XRD patterns.

3.2. *Electrochemical performance analysis*

In this study, PTLs with Pt coating thicknesses of 0.1 μm, 0.3 μm, 0.5 μm, and 0.7 μm were selected. According to Fig. 4(a), the polarization performance showed improvement with increasing the Pt coating's thickness. It should be noted that the linear increase in coating thickness did not result in a simple linear improvement in performance. When the Pt coating thickness was below 0.7 μm, the conductivity of the PTL was significantly enhanced by the electrodeposited Pt coating, as illustrated in Fig. S5. Additionally, the Tafel slope of the cell was reduced, as shown in Fig. 4(b), leading to an improvement in overall performance (Fig. 4 (a)). EIS Nyquist plots were fitted with the equivalent circuits model, as shown in Fig. 4(c). Where the points are measured data while the solid line is obtained by fitting with ZSimpWin software. The EIS also showed the promoting effect of the coating on the contact between PTL/CL within the PEMECs. According to the HFR obtained from EIS (Fig. 4(d)), the HFR significantly decreased when the coating thickness increased to about 0.5 μm. However, when the coating thickness increased from 0.5 μm to 0.7 μm, the polarization performance showed almost no change. These test results indicated that increasing the coating thickness is not always beneficial for performance in practical applications of PEMECs. Additionally, the hydrophilicity of the Ti felt was reduced with the presence of Pt coating (Fig. S6). Numerous studies had demonstrated that the hydrophilic PTL is more suitable for the PEMEC system. The increase in hydrophilicity contributes to easier water transport from the anode BP to the CL and membrane. Adequate water in the CL is beneficial to improve proton transfer, while adequate water in the membrane reduces ohmic resistance [51–53]. Therefore, there is a trade-off between the positive effect of Pt coating on PTL's conductivity and the negative effect of Pt coating on PTL's hydrophilicity and mass transfer in

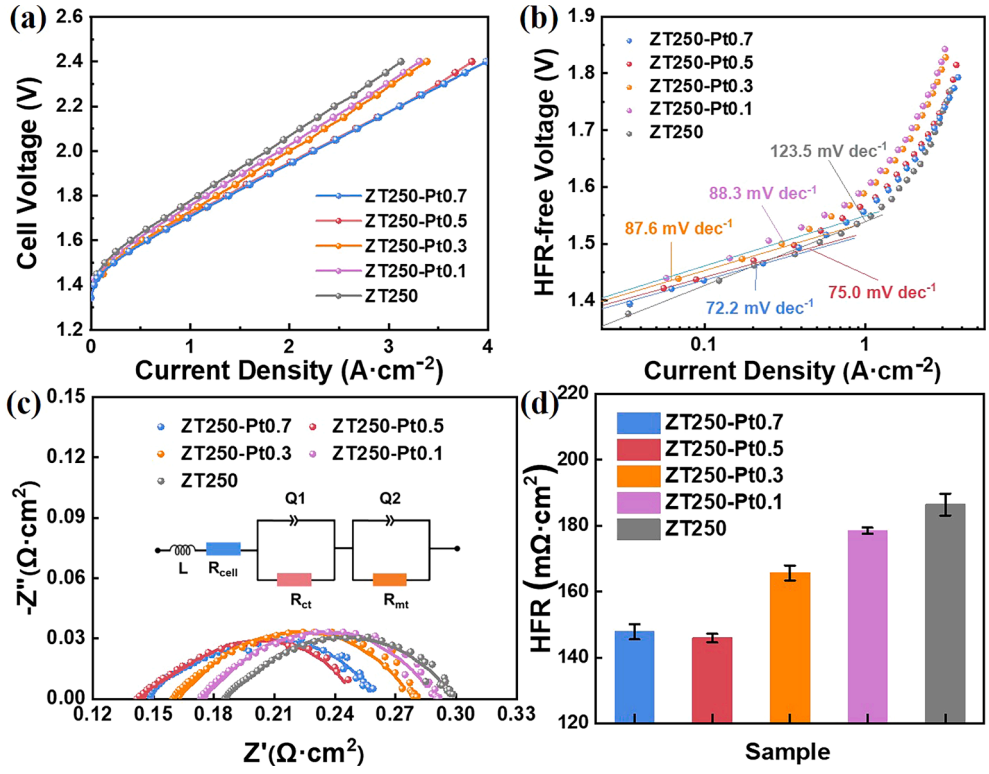

Fig. 4. (a) Polarization curves, (b) Tafel slopes of (c) EIS spectra, and (d) HFR of electrolyzers assembled with Ti-felt electrodeposited with different Pt coating.

the PEMECs.

Through secondary analysis of the polarization curves, the ohmic overpotential (Fig. 5(a)) and the kinetic overpotential (Fig. 5(b)) can be separated, and the total overpotential at different current densities (Fig. 5(c)) can be compared. The test results showed that with the increase in coating thickness, the kinetic overpotential during the PEMEC reaction showed a decreasing trend. Since there was no proton-conducting polymer like Nafion in the coated PTL, the Pt in the PTL was unlikely to act as an electrocatalyst and cannot cause a change in the kinetic overpotential [25]. More likely, this phenomenon was due to the introduction of the coating reducing the surface roughness of the PTL, thereby improving the interfacial contact between the CL and the PTL. This improvement in interfacial contact increased the density of active reaction sites, leading to a decrease in Tafel slope ((Fig. 4(b)) and a decrease in kinetic overpotential ((Fig. 5(b)). Comparing the η_{mt} in Fig. 4 (c), the excessively thick coating caused performance loss at 3 A cm^{-2}. Table S2 provides detailed values of the various overpotentials at 3 A cm^{-2} for each sample. This phenomenon indicated that an excessively thick coating will cause mass transfer issues, especially at high current densities.

3.3. Mass transfer enhancement

To address the mass transfer issue of ZT250-Pt0.7, ordered water channels were successfully constructed on the surface via laser ablation technique, and the structure of ZT250-Pt0.7-Waterchannel is presented in Fig. S7. Combining a transparent electrolyzer with an optical microscope system (Fig. S2), the bubble transfer behavior of the PTL with water channels was directly observed at a high current density of 3 A cm^{-2}. When using ZT250-Pt0.7 as the anode PTL, the unfavorable conduction of Ti felts for bubbles were clearly observed (Fig. 6(a_1)), where small bubbles continued to grow and slow down the transfer rate. In contrast, the ZT250-Pt0.7-Waterchannel with ordered pores produced bubbles that were finer and did not over-aggregate (Fig. 6(a_2)), resulting in a faster transfer rate. As shown in Fig. 6(a), the polarization performance of the ZT250-Pt0.7-Waterchannel at low current densities decreased, which may be due to the reduced contact area between the ZT250-Pt0.7-Waterchannel with straight-through pores and the CL, resulting in a lower utilization of the catalyst. However, at high current densities, its performance significantly increased. According to EIS analysis, the HFR was increased by the introduction of pores, as shown in Fig. 6(b), which may be due to the introduction of straight-through pores causing an increase in interface contact issues. The fitted EIS curve shows that a smaller diffusion resistance is observed for samples with water channels compared to the ZT250-Pt0.7. The specific fitting parameters can be seen in Table S3. The overpotential at 3 A cm^{-2} of ZT250-Pt0.7 and ZT250-Pt0.7-Waterchannel was presented in Fig. 6(c). Compared with the original sample, the ohmic overpotential (Fig. S7a) and kinetic overpotential (Fig. S7b) of ZT250-Pt0.7-Waterchannel both increased by about 25 mV and 43 mV, respectively, by no more than 15 %. However, the mass transfer overpotential decreased by about 87 mV, which is roughly 46 % lower than the original. It suggests that the effect of mass transfer overpotential on the polarization curve was more pronounced at high current densities. Therefore, despite the slight increase in ohmic and kinetic overpotential caused by the construction of water channels, the comprehensive performance was improved. Aging tests were performed on both (Fig. S8(c)), showing that water channels do not destabilize the PTL. This finding aligns with the stability tests done with and without pores in the electrolyzer [54]. In conclusion, the construction of water channels was highly effective for improving the performance of ZT250-Pt0.7. This strategy holds promising prospects for future practical applications.

3.4. PTL's degradation study

To investigate the effect of Pt coating on the PTL's degradation of PEMECs, the aging experiment was conducted in the three-electrode system for 100 h (Fig. 7(a)). Before conducting aging tests, polarization performance tests were carried out and the initial polarization performance of ZT250 and ZT250 Pt0.5 is shown in Fig. 7(b), labeled as ZT250-BoT and ZT250 Pt0.5-BoT, respectively. It can be seen that the polarization performance difference between the coating and non-

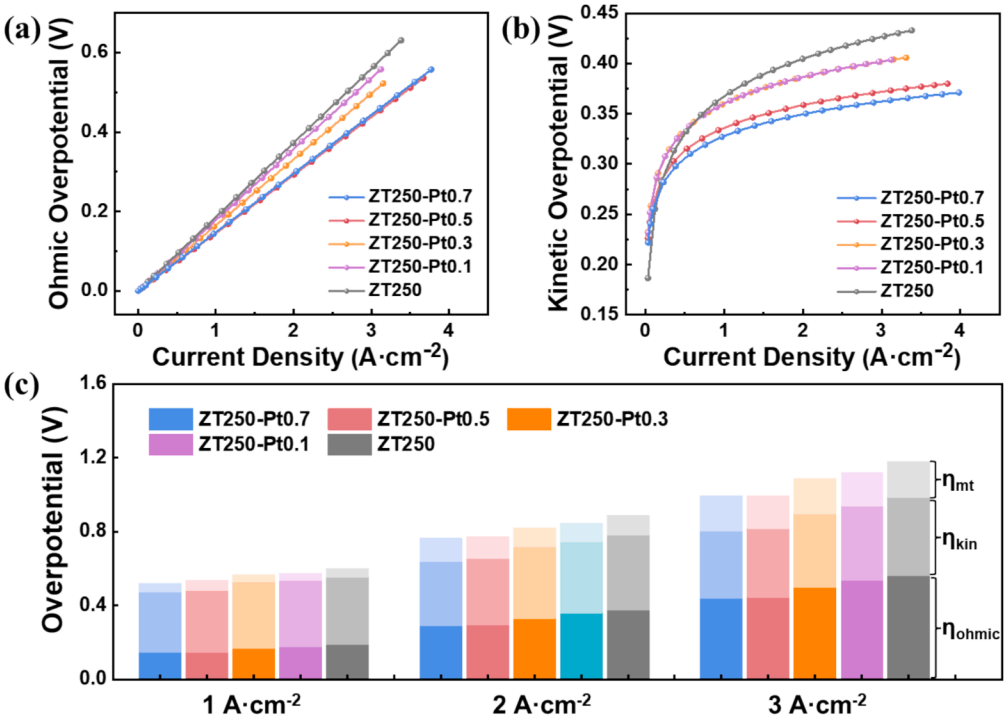

Fig. 5. (a) Ohmic overpotential, (b) kinetic overpotential and (c) comparison of overpotential of electrolyzers assembled with Ti-felt electrodeposited with different Pt coating.

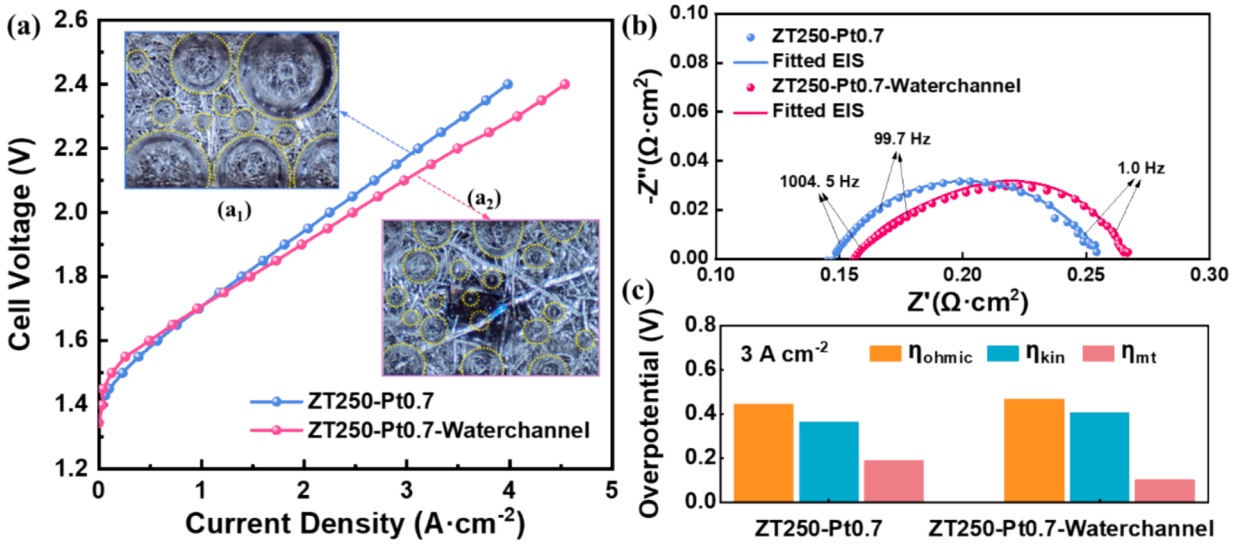

Fig. 6. Performance comparison of ZT250-Pt0.7 and ZT250-Pt0.7-Waterchannel in terms of (a) polarization performance, (b) EIS, and (c) overpotential. Fig. (a_1) and (a_2) represent the optical images of bubble transfer observed in a transparent electrolyzer, at a current density of 3 A cm^{-2}.

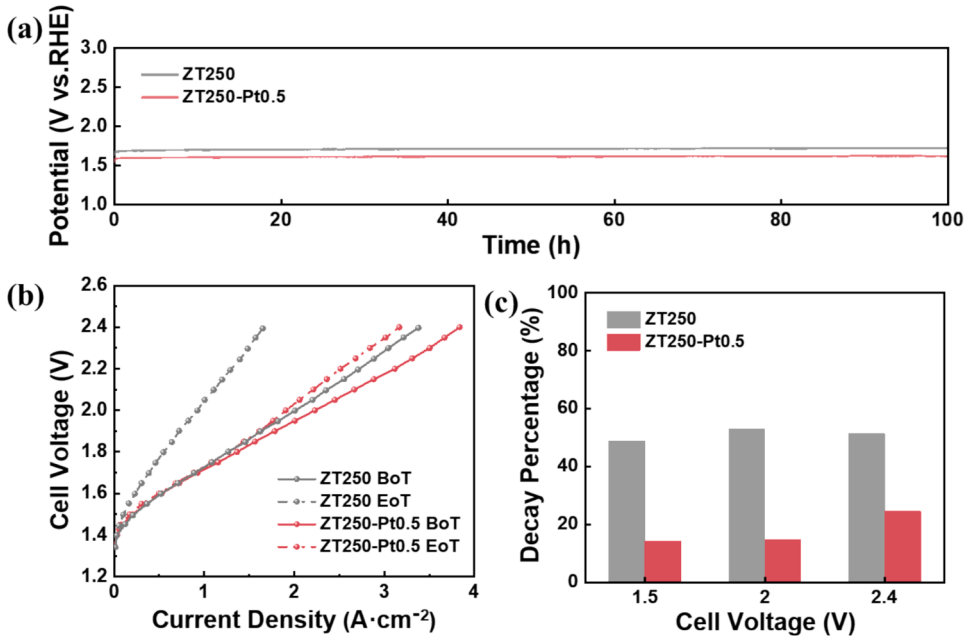

Fig. 7. (a) Aging of ZT250 and ZT250-Pt0.5 for 100 h, (b) polarization curves of electrolyzers using pristine and aged PTL, (c) percentage attenuation at different voltages after PTL's aging test.

coating begins to show when current density exceeds 1 A cm^{-2}. As the current density further increases, the difference became more pronounced. Subsequently, the PTLs after aging test were assembled in PEMECs and the polarization performance was tested again, labeled as ZT250-EoT and ZT250 Pt0.5-EoT. As shown in Fig. 7(b), the attenuation of ZT250 was significant, and its polarization performance was already less than half of its initial performance. In contrast, the attenuation degree of ZT250 Pt0.5 was effectively alleviated, and the polarization performance can reach about 80 % of the initial performance. The voltage decay rate of the electrolyzer at three representative voltages (1.5 V, 2 V and 2.4 V) was further analyzed (Fig. 7(c)). The uncoated ZT250 sample showed a high decay rate of about 50 % at multiple voltage points, indicating a significant performance degradation under these conditions. In contrast, the ZT250-Pt0.5 with Pt coating showed a decay rate of less than 20 % at the voltage points of 1.5 V and 2.0 V. Although the decay rate increased at the voltage point of 2.4 V, it still did not exceed 25 %. A similar trend is shown in the overpotential analysis (Fig. S9), with increases observed in ohmic overpotential, kinetic overpotential, and mass transfer overpotential for the ZT250, with distributions increasing by approximately 40 mV, 90 mV, and 140 mV. These results indicated that the degradation of Ti-based PTLs was slowed down by the addition of Pt coating. This finding is crucial for understanding and improving the long-term stability and reliability of PEMECs in practical applications, as the addition of the Pt coating provides an effective strategy for enhancing the durability of the PEMECs system.

In order to provide an in-depth analysis of the degradation behavior of PTLs, XPS was utilized to investigate the changes in PTL's chemical structure before and after the aging test. As shown in Fig. 8(a), pristine ZT250 exhibited peaks at 454.1 eV, corresponding to the $Ti^{0/II}$ $2p_{3/2}$

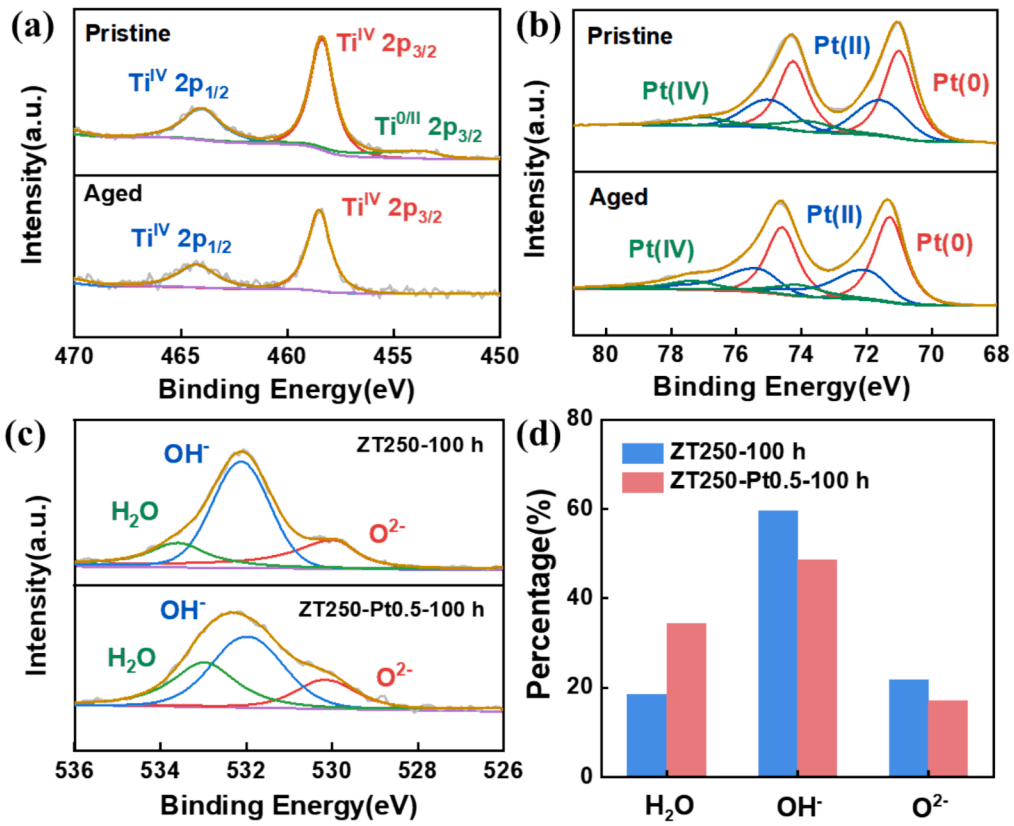

Fig. 8. (a) Comparison of Ti 2p XPS spectra before and after ZT250 aging test, (b) comparison of Pt 4f XPS spectra before and after ZT250-Pt0.5 aging test, (c) comparison of O 1s XPS spectra after aging test, (d) proportion of O 1s composition after aging test.

low-valence state, which disappeared after the aging test, indicating complete oxidation of all low-valence Ti species. It suggested the weak anti-oxidation capability of pristine ZT250. In contrast, Fig. 8(b) shows minimal change in the Pt 4f spectra of ZT250-Pt0.5 before and after the aging test. After aging for 100 h, only 2.7 % of Pt (0) was oxidized to a higher valence state, demonstrating the excellent corrosion resistance and anti-oxidation performance of ZT250-Pt0.5. The specific component changes are shown in Table S4. The O 1 s spectra in Fig. 8(c) reveal distinct peaks for H_2O, OH^-, and O^{2-} species. It had been shown in the reference [55] that the content of O^{2-} can be used to assess its anti-oxidant capacity. After the aging test, the comparison of O 1 s is shown in Fig. 8(d), and the O^{2-} content in ZT250-Pt0.5 was significantly lower than that of ZT250, further confirming its superior anti-oxidation performance. Specific compositional changes are shown in Table S5.

4. Conclusion

In conclusion, this study elucidated the impact of different Pt-coated Ti felts as anode PTL on the electrochemical performance of PEMECs, revealing a critical coating amount for cost-effective maximization of performance. The experimental analysis demonstrated that an excessive increase in coating thickness can lead to an increase in mass transfer resistance at high current densities, hindering gas–liquid transport in the Ti felt and limiting the improvement of PEMECs performance. The employment of laser-ablated ordered water channels on ZT250-Pt0.7 provided a simple and feasible solution to enhance mass transfer efficiency at high current densities. Furthermore, the Pt coating significantly enhanced the operational stability of PEMECs, which is crucial for the commercial application of coated Ti felts in PEMECs system. The findings of this study provide new insights into the design and manufacturing of electrolysis equipment in the hydrogen industry, offering a reference for achieving more cost-effective hydrogen production technologies.

CRediT authorship contribution statement

Xiuyue Wang: Writing – original draft, Methodology, Investigation, Formal analysis, Data curation, Conceptualization. **Jiexin Zou:** Writing – review & editing, Resources, Funding acquisition. **Zhen Zhang:** Writing – review & editing, Supervision, Conceptualization. **Cenkai Zhao:** Writing – review & editing, Methodology, Investigation. **Min Wang:** Writing – review & editing, Supervision, Project administration, Conceptualization. **Mingbo Wu:** Writing – review & editing, Supervision, Resources.

Declaration of competing interest

The authors declare that they have no known competing financial interests or personal relationships that could have appeared to influence the work reported in this paper.

Acknowledgments

This work was financially supported by the National Natural Science Foundation of China (Nos. 22208376, UA22A20429), Qingdao New Energy Shandong Laboratory Open Project (QNESL OP 202303), Shandong Provincial Natural Science Foundation (No. ZR2023LFG005) Shandong Postdoctoral Science Foundation (SDBX202302037) and the Qingdao Postdoctoral Applied Research Projects (QDBSH20240101050). M. Wang acknowledges the support from Jinan Ourui Industry Co., Ltd.

Appendix A. Supplementary data

Supplementary data to this article can be found online at https://doi.org/10.1016/j.fuel.2024.133559.

Data availability

Data will be made available on request.

References

[1] Jiao K, Xuan J, Du Q, Bao Z, Xie B, Wang B, et al. Designing the next generation of proton-exchange membrane fuel cells. Nature 2021;595(7867):361–9. https://doi.org/10.1038/s41586-021-03482-7.

[2] Fan L, Deng H, Zhang Y, Du Q, Leung DYC, Wang Y, et al. Towards ultralow platinum loading proton exchange membrane fuel cells. Energy Environ Sci 2023;16(4):1466–79. https://doi.org/10.1039/D2EE03169H.

[3] Wang M, Teng J, Zaman S, Zhang S, Chen X, Zhang K, et al. Optimized mass transfer in a Pt-based cathode catalyst layer for PEM fuel cells. Green Chem 2024;26(8):4432–48. https://doi.org/10.1039/D3GC05033E.

[4] Zhao W, Zaman S, Kong S, Liu M, Zou J, Zhang Z, et al. Optimization strategies and diagnostic techniques for water management in proton exchange membrane fuel cells. Green Chem Eng 2024. https://doi.org/10.1016/j.gce.2024.03.003.

[5] Zou J, Huang H, Zaman S, Yao K, Xing S, Chen M, et al. Enhanced electrochemical hydrogen compression performance with a gradient water-retaining hybrid membrane. Chem Eng J 2023;457:141113. https://doi.org/10.1016/j.cej.2022.141113.

[6] Liu K, Wu T, Cheng X, Cao M, Wang X, Su J, et al. Technical and economic analysis of a pilot-scale hydrogen system: From production to application. Energy Convers Manage 2023;291:117218. https://doi.org/10.1016/j.enconman.2023.117218.

[7] Wang Y, Wang M, Yang Y, Kong D, Meng C, Zhang D, et al. Potential technology for seawater electrolysis: Anion-exchange membrane water electrolysis. Chem Catal 2023;3(7):100643. https://doi.org/10.1016/j.checat.2023.100643.

[8] Kojima H, Nagasawa K, Todoroki N, Ito Y, Matsui T, Nakajima R. Influence of renewable energy power fluctuations on water electrolysis for green hydrogen production. Int J Hydrogen Energy 2023;48(12):4572–93. https://doi.org/10.1016/j.ijhydene.2022.11.018.

[9] Ikuerowo T, Bade SO, Akinmoladun A, Oni BA. The integration of wind and solar power to water electrolyzer for green hydrogen production. Int J Hydrogen Energy 2024. https://doi.org/10.1016/j.ijhydene.2024.02.139.

[10] Chi J, Yu H. Water electrolysis based on renewable energy for hydrogen production. Chin J Catal 2018;39(3):390–4. https://doi.org/10.1016/S1872-2067(17)62949-8.

[11] Kang Z, Wang H, Liu Y, Mo J, Wang M, Li J, et al. Exploring and understanding the internal voltage losses through catalyst layers in proton exchange membrane water electrolysis devices. Appl Energy 2022;317:119213. https://doi.org/10.1016/j.apenergy.2022.119213.

[12] Kang Z, Wang M, Yang Y, Wang H, Liu Y, Mo J, et al. Performance improvement induced by membrane treatment in proton exchange membrane water electrolysis cells. Int J Hydrogen Energy 2022;47(9):5807–16. https://doi.org/10.1016/j.ijhydene.2021.11.227.

[13] Zhang S, Wang Z, Zhang R, He Y, Cen K. Comprehensive study and optimization of membrane electrode assembly structural composition in proton exchange membrane water electrolyzer. Int J Hydrogen Energy 2023;48(91):35463–76. https://doi.org/10.1016/j.ijhydene.2023.05.280.

[14] Prestat M. Corrosion of structural components of proton exchange membrane water electrolyzer anodes: A review. J Power Sources 2023;556:232469. https://doi.org/10.1016/j.jpowsour.2022.232469.

[15] Qiu C, Xu Z, Chen F-Y, Wang H. Anode engineering for proton exchange membrane water electrolyzers. ACS Catal 2024;14(2):921–54. https://doi.org/10.1021/acscatal.3c05162.

[16] Schuler T, Ciccone JM, Krentscher B, Marone F, Peter C, Schmidt TJ, et al. Hierarchically structured porous transport layers for polymer electrolyte water electrolysis. Adv Energy Mater 2020;10(2):1903216. https://doi.org/10.1002/aenm.201903216.

[17] Park SH, Koo J, Park Y-J, Jang S, Ryu HJ, Han H, et al. Uniformly scalable and stackable porous transport layer manufactured by tape casting and calendering for efficient water electrolysis. Chem Eng J 2024;481:148276. https://doi.org/10.1016/j.cej.2023.148276.

[18] Parra-Restrepo J, Bligny R, Dillet J, Didierjean S, Stemmelen D, Moyne C, et al. Influence of the porous transport layer properties on the mass and charge transfer in a segmented PEM electrolyzer. Int J Hydrogen Energy 2020;45(15):8094–106. https://doi.org/10.1016/j.ijhydene.2020.01.100.

[19] Siracusano S, Di Blasi A, Baglio V, Brunaccini G, Briguglio N, Stassi A, et al. Optimization of components and assembling in a PEM electrolyzer stack. Int J Hydrogen Energy 2011;36(5):3333–9. https://doi.org/10.1016/j.ijhydene.2010.12.044.

[20] Kim PJ, Lee JK, Lee CH, Fahy KF, Shrestha P, Krause K, et al. Tailoring catalyst layer interface with titanium mesh porous transport layers. Electrochim Acta 2021;373:137879. https://doi.org/10.1016/j.electacta.2021.137879.

[21] Mo J, Kang Z, Yang G, Retterer ST, Cullen DA, Toops TJ, et al. Thin liquid/gas diffusion layers for high-efficiency hydrogen production from water splitting. Appl Energy 2016;177:817–22. https://doi.org/10.1016/j.apenergy.2016.05.154.

[22] Kang Z, Yang G, Mo J, Li Y, Yu S, Cullen DA, et al. Novel thin/tunable gas diffusion electrodes with ultra-low catalyst loading for hydrogen evolution reactions in proton exchange membrane electrolyzer cells. Nano Energy 2018;47:434–41. https://doi.org/10.1016/j.nanoen.2018.03.015.

[23] Ito H, Maeda T, Nakano A, Kato A, Yoshida T. Influence of pore structural properties of current collectors on the performance of proton exchange membrane electrolyzer. Electrochim Acta 2013;100:242–8. https://doi.org/10.1016/j.electacta.2012.05.068.

[24] Kang Z, Schuler T, Chen Y, Wang M, Zhang F-Y, Bender G. Effects of interfacial contact under different operating conditions in proton exchange membrane water electrolysis. Electrochim Acta 2022;429:140942. https://doi.org/10.1016/j.electacta.2022.140942.

[25] Liu C, Carmo M, Bender G, Everwand A, Lickert T, Young JL, et al. Performance enhancement of PEM electrolyzers through iridium-coated titanium porous transport layers. Electrochem Commun 2018;97:96–9. https://doi.org/10.1016/j.elecom.2018.10.021.

[26] Borgardt E, Panchenko O, Hackemüller FJ, Giffin J, Bram M, Müller M, et al. Mechanical characterization and durability of sintered porous transport layers for polymer electrolyte membrane electrolysis. J Power Sources 2018;374:84–91. https://doi.org/10.1016/j.jpowsour.2017.11.027.

[27] Liu J, Liu H, Yang Y, Tao Y, Zhao L, Li S, et al. Efficient and stable proton exchange membrane water electrolysis enabled by stress optimization. ACS Cent Sci 2024;10(4):852–9. https://doi.org/10.1021/acscentsci.4c00037.

[28] Kang Z, Alia SM, Young JL, Bender G. Effects of various parameters of different porous transport layers in proton exchange membrane water electrolysis. Electrochim Acta 2020;354:136641. https://doi.org/10.1016/j.electacta.2020.136641.

[29] Stiber S, Balzer H, Wierhake A, Wirkert FJ, Roth J, Rost U, et al. Porous transport layers for proton exchange membrane electrolysis under extreme conditions of current density, temperature, and pressure. Adv Energy Mater 2021;11(33):2100630. https://doi.org/10.1002/aenm.202100630.

[30] Ahmed KW, Jang MJ, Park MG, Chen Z, Fowler M. Effect of components and operating conditions on the performance of PEM electrolyzers: A review. Electrochem 2022;3:581–612.

[31] Kazim AM. Exergoeconomic analysis of a PEM electrolyser at various operating temperatures and pressures. Int J Energy Res 2005;29(6):539–48. https://doi.org/10.1002/er.1073.

[32] Grigoriev SA, Millet P, Volobuev SA, Fateev VN. Optimization of porous current collectors for PEM water electrolysers. Int J Hydrogen Energy 2009;34(11):4968–73. https://doi.org/10.1016/j.ijhydene.2008.11.056.

[33] Tan A, Zhang Y, Shi X, Ju C, Liu P, Yang T, et al. The poisoning effects of Ti-ion from porous transport layers on the membrane electrode assembly of proton exchange membrane water electrolyzers. Chem Eng J 2023;471:144624. https://doi.org/10.1016/j.cej.2023.144624.

[34] Srour T, Kumar K, Martin V, Dubau L, Maillard F, Gilles B, et al. On the contact resistance between the anode and the porous transport layer in a proton exchange membrane water electrolyzer. Int J Hydrogen Energy 2024;58:351–61. https://doi.org/10.1016/j.ijhydene.2024.01.134.

[35] Rakousky C, Keeley GP, Wippermann K, Carmo M, Stolten D. The stability challenge on the pathway to high-current-density polymer electrolyte membrane water electrolyzers. Electrochim Acta 2018;278:324–31. https://doi.org/10.1016/j.electacta.2018.04.154.

[36] Sun S, Shao Z, Yu H, Li G, Yi B. Investigations on degradation of the long-term proton exchange membrane water electrolysis stack. J Power Sources 2014;267:515–20. https://doi.org/10.1016/j.jpowsour.2014.05.117.

[37] Liu C, Shviro M, Gago AS, Zaccarine SF, Bender G, Gazdzicki P, et al. Exploring the interface of skin-layered titanium fibers for electrochemical water splitting. Adv Energy Mater 2021;11(8):2002926. https://doi.org/10.1002/aenm.202002926.

[38] Minke C, Suermann M, Bensmann B, Hanke-Rauschenbach R. Is iridium demand a potential bottleneck in the realization of large-scale PEM water electrolysis? Int J Hydrogen Energy 2021;46(46):23581–90. https://doi.org/10.1016/j.ijhydene.2021.04.174.

[39] Kang Z, Mo J, Yang G, Li Y, Talley DA, Retterer ST, et al. Thin film surface modifications of thin/tunable liquid/gas diffusion layers for high-efficiency proton exchange membrane electrolyzer cells. Appl Energy 2017;206:983–90. https://doi.org/10.1016/j.apenergy.2017.09.004.

[40] Lee JK, Schuler T, Bender G, Sabharwal M, Peng X, Weber AZ, et al. Interfacial engineering via laser ablation for high-performing PEM water electrolysis. Appl Energy 2023;336:120853. https://doi.org/10.1016/j.apenergy.2023.120853.

[41] Jiang B, Yu L, Wu L, Mu D, Liu L, Xi J, et al. Insights into the impact of the Nafion membrane pretreatment pocess on vanadium flow battery performance. ACS Appl Mater Interfaces 2016;8(19):12228–38. https://doi.org/10.1021/acsami.6b03529.

[42] Karimi MB, Mohammadi F, Hooshyari K. Recent approaches to improve Nafion performance for fuel cell applications: a review. Int J Hydrogen Energy 2019;44(54):28919–38. https://doi.org/10.1016/j.ijhydene.2019.09.096.

[43] Wang M, Park JH, Kabir S, Neyerlin KC, Kariuki NN, Lv H, et al. Impact of catalyst ink dispersing methodology on fuel cell performance using in-situ X-ray scattering. ACS Appl Energy Mater 2019;2(9):6417–27. https://doi.org/10.1021/acsaem.9b01037.

[44] Bernt M, Hartig-Weiß A, Tovini MF, El-Sayed HA, Schramm C, Schröter J, et al. Current challenges in catalyst development for PEM water electrolyzers. Chem Ing Tech 2020;92(1–2):31–9. https://doi.org/10.1002/cite.201900101.

[45] Oh H-S, Nong HN, Reier T, Gliech M, Strasser P. Oxide-supported Ir nanodendrites with high activity and durability for the oxygen evolution reaction in acid PEM water electrolyzers. Chem Sci 2015;6(6):3321–8. https://doi.org/10.1039/C5SC00518C.

[46] Niu S, Li S, Du Y, Han X, Xu P. How to reliably report the overpotential of an electrocatalyst. ACS Energy Lett 2020;5(4):1083–7. https://doi.org/10.1021/acsenergylett.0c00321.
[47] Liang Y, Li Y, Wang H, Zhou J, Wang J, Regier T, et al. Co_3O_4 nanocrystals on graphene as a synergistic catalyst for oxygen reduction reaction. Nat Mater 2011;10(10):780–6. https://doi.org/10.1038/nmat3087.
[48] Lee JK, Anderson G, Tricker AW, Babbe F, Madan A, Cullen DA, et al. Ionomer-free and recyclable porous-transport electrode for high-performing proton-exchange-membrane water electrolysis. Nat Commun 2023;14(1):4592. https://doi.org/10.1038/s41467-023-40375-x.
[49] Schuler T, Schmidt TJ, Büchi FN. Polymer electrolyte water electrolysis: Correlating performance and porous transport layer structure: Part II. Electrochemical performance analysis. J Electrochem Soc 2019;166(10):F555. https://doi.org/10.1149/2.1241908jes.
[50] Xie Y, Yuan C. Visible-light responsive cerium ion modified titania sol and nanocrystallites for X-3B dye photodegradation. Appl Catal B-environ 2003;46(2):251–9. https://doi.org/10.1016/S0926-3373(03)00211-X.
[51] Wang Q, Zhou Z, Ye K, Hu M, Hu X, Wang S, et al. The effect of pretreatment and surface modification of porous transport layer (PTL) on the performance of proton exchange membrane water electrolyzer. Int J Hydrogen Energy 2024;53:163–72. https://doi.org/10.1016/j.ijhydene.2023.12.057.
[52] Zhao B, Lee C, Lee JK, Fahy KF, LaManna JM, Baltic E, et al. Superhydrophilic porous transport layer enhances efficiency of polymer electrolyte membrane electrolyzers. Cell Rep Phys Sci 2021;2(10):100580. https://doi.org/10.1016/j.xcrp.2021.100580.
[53] Yuan S, Zhao C, Mei X, Shen S, Wang Q, Yan X, et al. Bubble management in PEM water electrolysis via imprinting patterned grooves on catalyst layer. Int J Heat Mass Transfer 2023;212:124249. https://doi.org/10.1016/j.ijheatmasstransfer.2023.124249.
[54] Zhu K, Zhang H, Zhu L, Tian T, Tang H, Lu X, et al. Porous transport layers with laser micropatterning for enhanced mass transport in PEM water electrolyzers. Nano Lett 2024;24(34):10656–63. https://doi.org/10.1021/acs.nanolett.4c03112.
[55] Wang X, Luo H, Cheng H, Yue L, Deng Z, Yao J, et al. Investigation on the performance of Pt surface modified Ti bipolar plates in proton exchange membrane water electrolyzer. Appl Energy 2024;357:122517. https://doi.org/10.1016/j.apenergy.2023.122517.